Electronic Supplementary Material (ESI) for Nanoscale.
This journal is © The Royal Society of Chemistry 2016

Electronic Supplementary Information (ESI)

Rationally Encapsulated Gold Nanorods Improving both Linear and Nonlinear Photoacoustic Imaging Contrast *in Vivo*

Fei Gao,[‡,a] Linyi Bai,[‡,b] Siyu Liu,[a] Ruochong Zhang,[a] Jingtao Zhang,[b] Xiaohua Feng,[a] Yuanjin Zheng,*[,a] and Yanli Zhao*[,b,c]

[a]School of Electrical and Electronic Engineering, Nanyang Technological University, 50 Nanyang Avenue, Singapore 639798. Email: yjzheng@ntu.edu.sg
[b]Division of Chemistry and Biological Chemistry, School of Physical and Mathematical Sciences, Nanyang Technological University, 21 Nanyang Link, Singapore 637371. E-mail: zhaoyanli@ntu.edu.sg
[c]School of Materials Science and Engineering, Nanyang Technological University, 50 Nanyang Avenue, Singapore 639798
[‡]These authors contributed equally to this work.

Email: zhaoyanli@ntu.edu.sg; yjzheng@ntu.edu.sg

1. Instruments

1.1 Thermogravimetric analysis (TGA) and Fourier transform infrared (FT-IR) experiments

TGA was performed on a TGA 500 thermogravimetric analyzer by heating the samples at 20 ºC min^{-1} to 1000 ºC in a nitrogen atmosphere (60 mL/min). FTIR spectra (KBr, Aldrich) were measured with an SHIMADZU IR Prestige-21 spectrometer. Samples were packed firmly to obtain transparent films.

1.2 XPS measurement

X-Ray photoelectric spectroscopy (XPS) was carried out on a Phoibos 100 spectrometer.

1.3 Transmission electron microscopy (TEM)

TEM images were obtained on JEM-1400 (JEOL) at an acceleration voltage of 100 kV.

1.4 UV absorption and confocal laser microscopy (CLSM)

Absorption spectra were recorded on UV-3600 UV−vis−NIR spectrophotometer (Shimadzu). Confocal laser microscopy (CLSM) images were acquired by a Leica TCS confocal microscope with a Nikon Eclipse TE2000-S objective (60× oil).

2. Preparation of dispersed Au NRs and two hybrids

Chloroauric acid ($HAuCl_4 \bullet 3H_2O$) employed for Au NRs was commercially available and used without further purifications unless specifically mentioned. The two hybrids Au NR@ZnTPP and Au NR@PVP+ZnTPP were synthesized following the literature procedures[S1-S3] with some modifications as shown below.

2.1 Au NRs

Briefly, gold nanoparticle seed solution was prepared first by adding an ice-cold solution (0.6 mL) of sodium borohydride (10 mM) to chloroauric acid solution (10 mL of 2.5×10^{-4} M) prepared in cetyl trimethylammonium bromide (CTAB, 0.1 M) solution under vigorous stirring. The yellow color changed immediately to brown, indicating the formation of gold nanoparticle seeds. Stirring was continued further for 10 min. These seeds were used for the synthesis of gold nanorods. Briefly, the following solutions were added to a 200 mL conical flask in the following order: 95 mL of 0.1 M CTAB solution, 1 mL of 10 mM silver nitrate solution, and 5 mL of 10 mM chloroauric acid. To this solution was added ascorbic acid (0.55 mL, 0.1 M), and the mixture was homogenized by shaking gently. Finally, the seed solution (0.12 mL) was added, and the entire solution was mixed and left undisturbed overnight (14-16 h). The violet-brown colored gold nanorod solution prepared was purified by centrifugation to remove excess CTAB (twice at 14000 rpm, 10 min each).

2.2 Au NR@ZnTPP

To load ZnTPP onto Au NRs, ZnTPP (5.0 mg) was firstly dispersed in DMF (5 mL) and then transferred into ethanol (45 mL) with pH>7. Subsequently, the mixture of Au NR solution (3 mL) and this ZnTPP dispersion (12 mL) was stirred at 35 ºC for overnight. After which, the reaction was centrifuged down and the supernatant was kept for further analysis. The obtained product, Au NR@ZnTPP, was washed by deionized water for 3 times.

The ZnTPP layer on Au NRs can be observed by TEM. The detailed loading percentage was tracked by measuring the difference between the absorbance of the ZnTPP dispersion (volume ratio of DMF and ethanol is 1:9) before mixing with Au NRs and the supernatant obtained after centrifuging for overnight, and by TGA. The concentration of ZnTPP loaded was calculated using the ZnTPP dispersion calibration curve.

2.3 Au NR@PVP+ZnTPP

In the preparation of Au NRs, CTAB surfactant was used to stabilize the Au NR dispersion. To introduce polyvinylpyrrolidone (PVP) as the surfactant, an exchange progress was carried out, where the mixture of PVP and Au NRs stabilized with CTAB was stirred at 60 ºC for 4 hours. The resulted mixture was diluted by deionized water and then centrifuged down. The saturated PVP-covered Au NRs were obtained after repeating the centrifugation for 4-5 times.

The saturated PVP-covered Au NR solution (0.5 mL) was mixed with deionized water (1.5 mL). A 11-mercaptoundecanoic acid stock solution (10 mM, 0.1 mL) was added to methanol (1.9 mL). Then, the acid solution (1 mL) was added dropwise to the PVP-covered Au NRs over a period of 15-20 minutes. After which, the solution was mixed with abovementioned ZnTPP solution (8 mL) under stirring for an additional 6 hours. A thick layer covered on the surface of Au NRs can be found by TEM.

2.4 Comparative experiments for Au NRs and two hybrids in aqueous solution containing PBS

To further characterize the photophysical stability of Au NRs and two hybrids containing ZnTPP, a comparative experiment in PBS solution was performed for evaluating their suitability in cell incubation studies.

For the preparation of three samples in PBS solution, the three samples were separately placed in a vial and dipped in PBS (2 mL, pH = 7.4, standard buffer solution from Sigma) at room temperature. Then, the mixture was stirred for overnight. Their UV absorbance was analyzed by UV-Vis spectrophotometry with the help of a calibration curve.

3. Physical properties of Au NRs and two hybrids

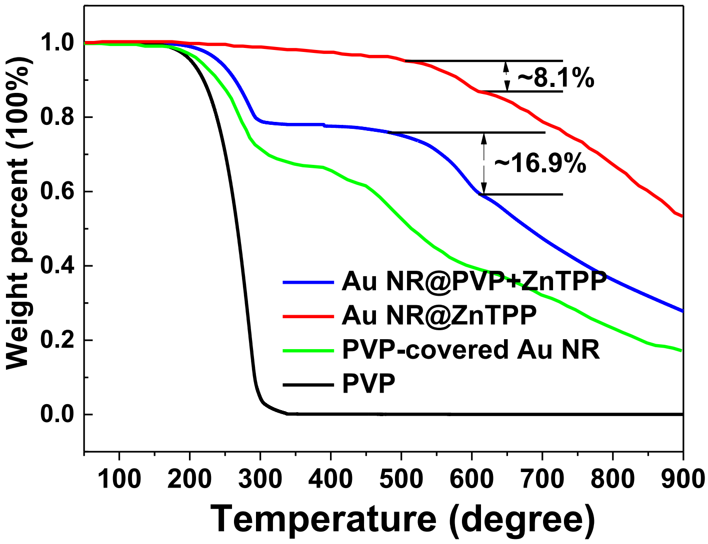

Figure S1. TGA curves of Au NRs, PVP-covered Au NRs, Au NR@ZnTPP, and Au NR@PVP+ZnTPP.

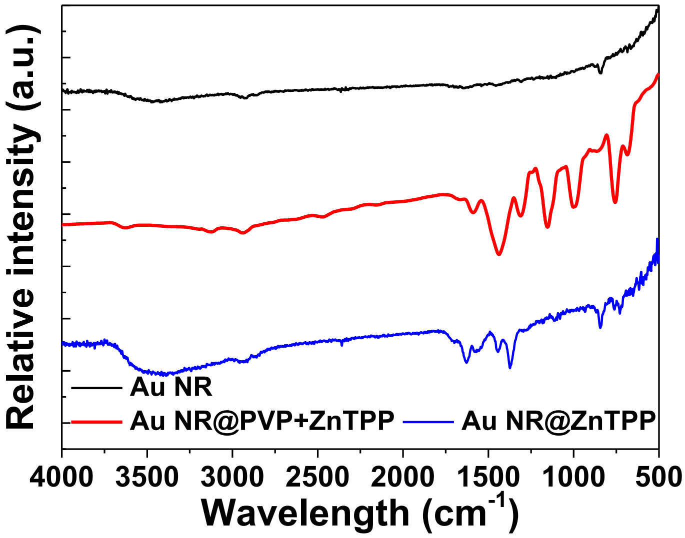

Figure S2. FTIR spectra of Au NRs, Au NR@ZnTPP, and Au NR@PVP+ZnTPP.

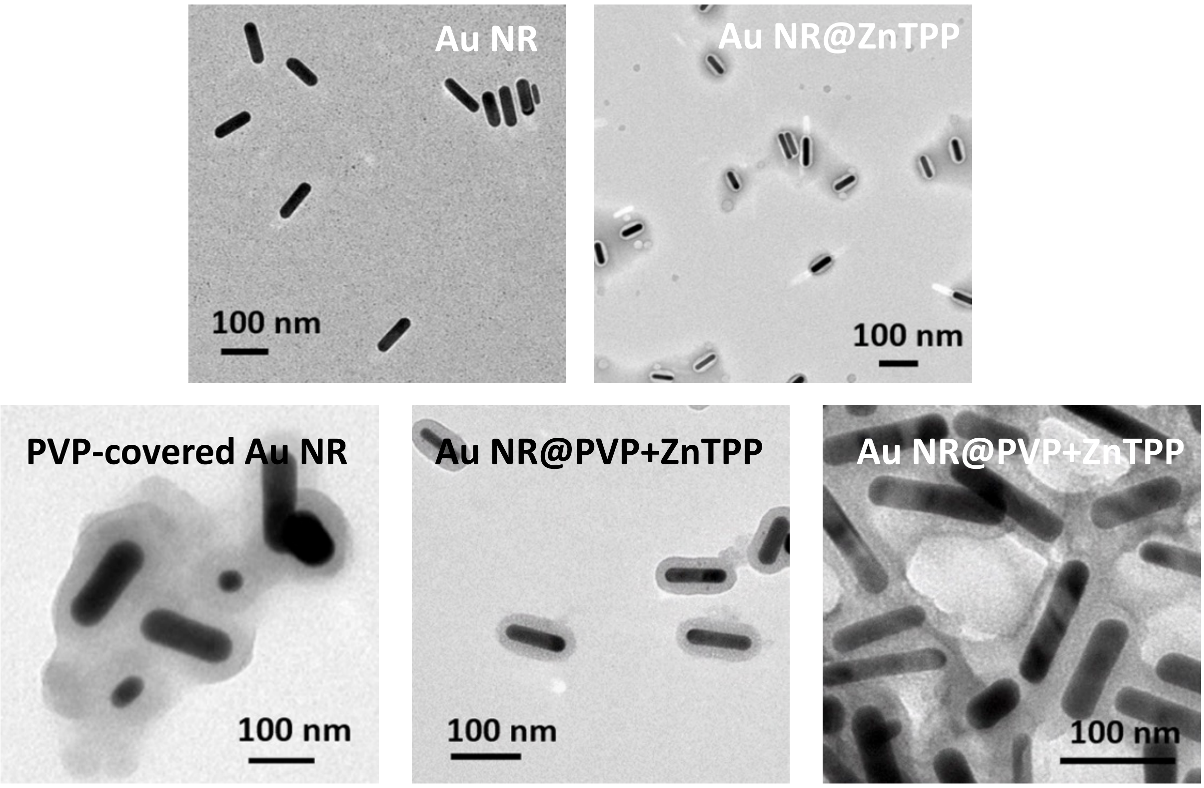

Figure S3. TEM images of Au NRs, PVP-covered Au NRs, Au NR@ZnTPP, and Au NR@PVP+ZnTPP in aqueous solution containing PBS.

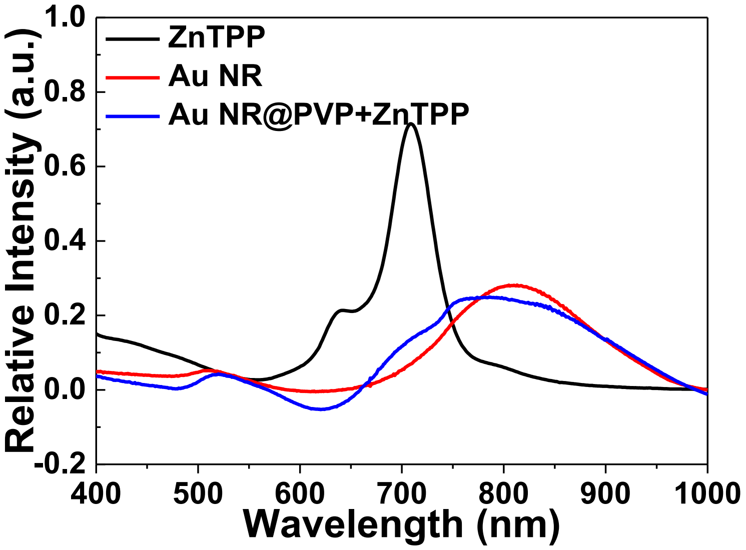

Figure S4. UV absorbance spectra of ZnTPP, Au NRs, and Au NR@PVP+ZnTPP in aqueous solution containing PBS.

4. *In vitro* cytotoxicity study

The biocompatibility of two hybrids was quantitatively investigated by using standard

3-(4,5-dimethylthiazol-2-yl)-2,5-diphenyltetrazolium bromide (MTT) assay based on the proliferations of HeLa cells. Briefly, the cells were seeded in 96-well plates (100 µL medium) and incubated. When the cell confluence reached around 60−70%, the medium was replaced with fresh one (90 µL), and then two hybrid suspensions (10 µL each) with various concentrations were added, in which the initial concentration was the same as that used in UV absorbance measurements, and the rest concentrations were obtained by diluting the solutions from 1 to 5 times. After incubation for 24 h or 48 h, optical densities of the samples were measured using a microplate reader (infinite M200, TECAN) at 490 nm. The cell viability (%) was calculated based on the following equation: $(A_{sample}/A_{control}) \times 100$, where A_{sample} and $A_{control}$ represent the absorbance of the sample and control groups, respectively.

5. Theory of quasi-CW nonlinear PA imaging

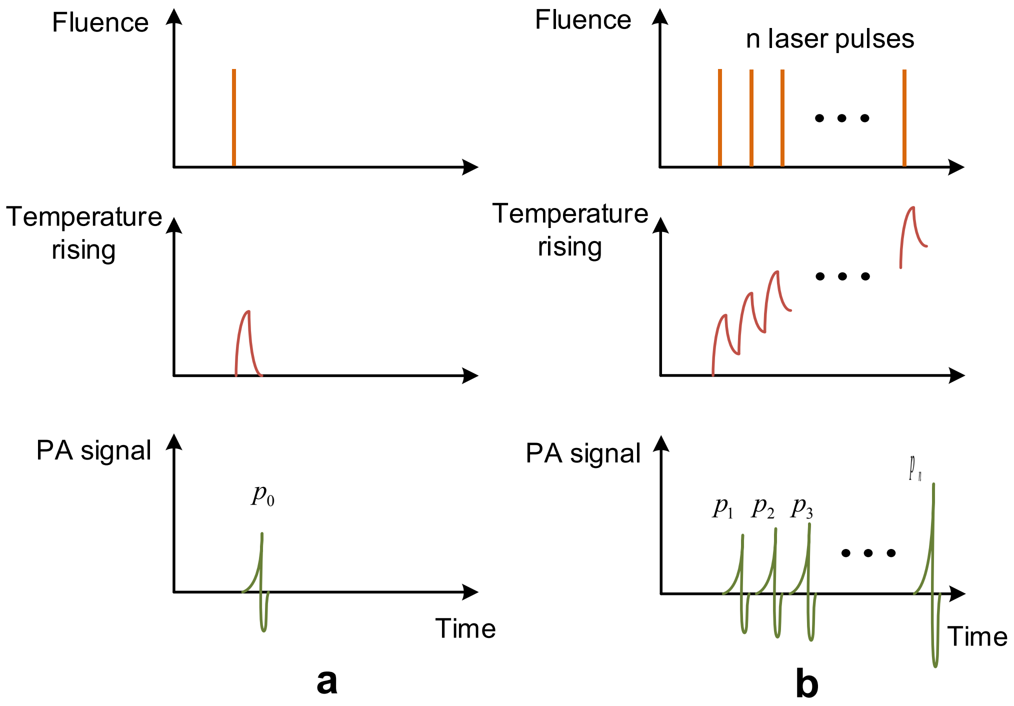

Figure S5. Fluence pattern, temperature change and PA signal waveform of (a) conventional single laser pulse induced linear PA effect, and (b) multiple laser pulse induced quasi-CW nonlinear PA effect with heat accumulation.

For conventional PA imaging technique, an ultrashort laser pulse with nanosecond pulse-width is used to induce transient temperature rise from the optical absorber, which is linearly proportional to the optical absorption coefficient. A dipolar PA signal could be generated following the thermoelastic expansion and contraction (Figure S5a). The analytical expression of the linear PA signal P_0 is:

$$\text{Linear PA}: p_0 = \Gamma_0 \eta_{th} \mu_a F \tag{S1}$$

where Γ_0 is the Gruneisen coefficient at the ambient temperature, η_{th} is the conversion efficiency from heat to pressure, μ_a is the optical absorption coefficient, and F is the light fluence. This is the governing equation for conventional PA imaging based on linear optical absorption.

On the other hand, the quasi-CW nonlinear PA signal based on multiple laser pulse illumination could exhibit larger amplitude, which could be majorly caused by the increased Gruneisen coefficient (thermal expansion coefficient increased) due to the heat accumulation and temperature rise of the object during the quasi-CW laser illumination and heating. The analytical expression of the *n* PA signal P_n could be derived as:

$$\text{Nonlinear PA: } p_n = p_0 + \overbrace{b\eta_{th}^2\mu_a^2F^2\tau_{th}^2\left\{1-\left[1+\frac{(n-1)(\tau_{th}-\tau_{pi})}{\tau_{th}}\right]e^{-\frac{(n-1)(\tau_{th}-\tau_{pi})}{\tau_{th}}}\right\}}^{\text{Nonlinear enhancement term}},\ \tau_{th}-\tau_{pi}>0 \quad \text{(S2)}$$

where *b* is the coefficient relating the absorbed thermal energy to the Gruneisen parameter change, $\tau_{th} = d^2/\alpha$ is the thermal relaxation time (*d* is the size of the optical absorber, and α is the thermal diffusivity of the optical absorber), and τ_{pi} is the laser pulse interval. Compared with Eq. (S1) for the conventional linear PA, the quasi-CW nonlinear PA signal P_n shows the nonlinearity governed by the Gruneisen term increase due to the heat accumulation during the *n* laser pulse illumination. It describes the Gruneisen coefficient increase due to the temperature rise of the object and saturation following heat accumulation during the multiple laser pulse illumination. It should be noted that τ_{th} - $\tau_{pi} > 0$, so that within two consequent laser pulses, the accumulated heat by the first laser pulse doesn't totally dissipate before the arrival of the second laser pulse. When τ_{th} - $\tau_{pi} = 0$ or $n = 1$, Eq. (S2) goes back to $P_n = P_0$ on account of no heat accumulation between consecutive pulses or by only single pulse.

6. Nonlinear PA imaging *in vitro*

The experimental setup for nonlinear PA imaging in vitro is shown in Figure S6. The input multiple pulse signals are generated by a function generator (Tektronix) that is connected to a high-power pulsed laser diode system (Quantel Laser Diode Illuminator; wavelength: 808 nm; pulse width: 100 ns; rep. rate: up to 10 kHz; pulse interval: > 100 μs; maximum pulse energy: 1 mJ). The output of the pulsed laser diode is coupled into a multi-mode fiber. Then, the output light from the fiber is collimated and focused by condenser lens on the sample. Meanwhile, a beam splitter and a photodiode are utilized to monitor the laser intensity variation. An ultrasound transducer (V303SU, Olympus) with 1 MHz central frequency is placed close to the sample to detect both linear and nonlinear PA signals. The samples are made of microtubes filled with the synthesized systems. Both of the sample and transducer are immersed in water tank for optimum optical and acoustic coupling. The multiple nonlinear PA signals are firstly amplified by a low-noise amplifier (5662, Olympus) with 54 dB gain, which is then stored by an oscilloscope (LeCroy) with 100 MSPS sampling rate. The optical path and ultrasound transducer are mounted on a 2D mechanical scanning stage that enables point-to-point raster scanning covering the sample to render 2D linear and nonlinear PA images.

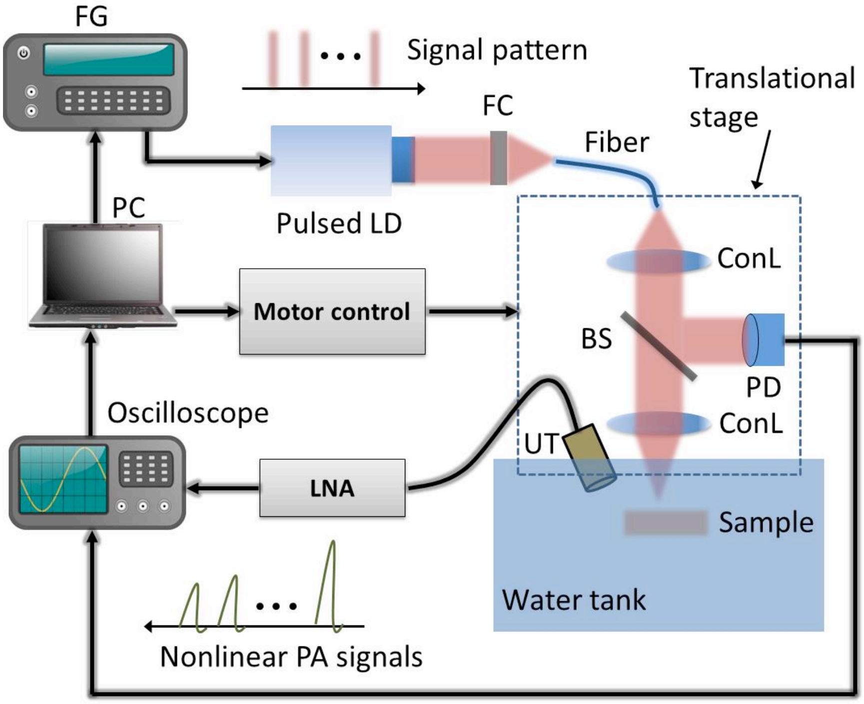

Figure S6. Schematic presentation of the experimental setup. FC: function generator; PC: personal computer; LD: laser diode; FC: fiber coupler; ConL: condenser lens; BS: beam splitter; PD: photodiode; UT: ultrasound transducer; LNA: low-noise amplifier.

7. Nonlinear PA imaging *in vivo*

The *in vivo* imaging setup shown in Figure S7 includes a water tank with a hole cut at the bottom, which was sealed by transparent polymer membrane as the imaging window for both optimum optical and optimum acoustic coupling. The abdomen of the rat was treated by ultrasound gel after removing the hair in the region of interest. Then, the rat was tightly attached to the membrane below the water tank. The objective lens and ultrasound transducer were assembled and mounted to a mechanical scanner to sense the PA signals at each scanning point with scanning step of 50 µm to reconstruct both linear and nonlinear PA images.

This study conforms to the Guide for the Care and Use of Laboratory Animals published by the National Institutes of Health, USA and protocol approved by the Institutional Animal Care and Use Committee (IACUC), Nanyang Technological University. Ten-week-old rat was used for this in vivo imaging study. The animal was anesthetized with isofluorane (1.5%).

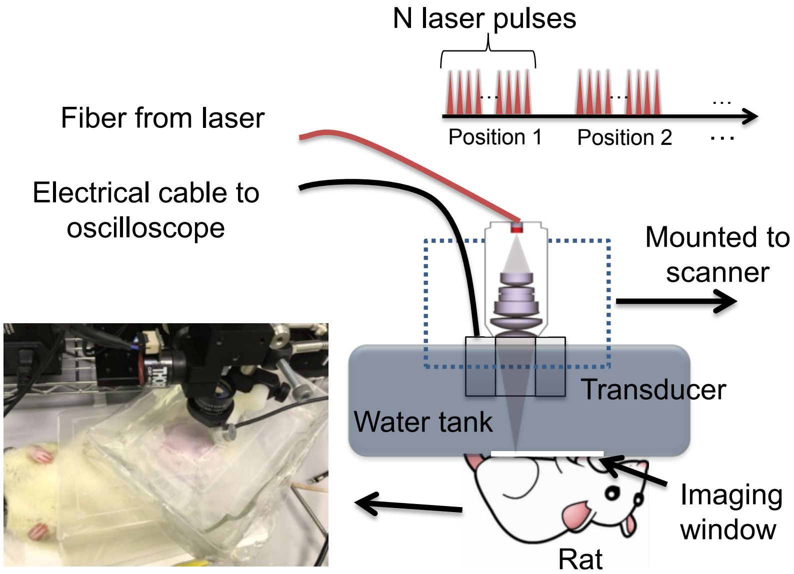

Figure S7. Diagram of the *in vivo* animal imaging including water tank with transparent membrane coupling.

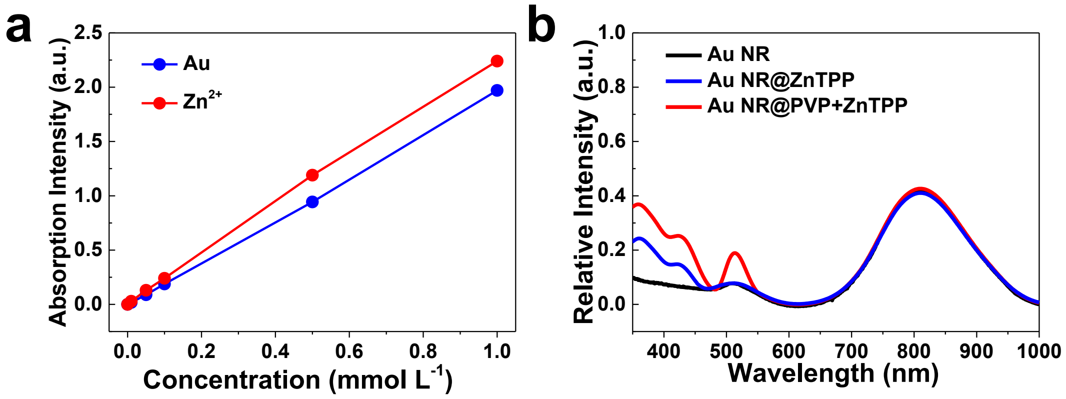

Figure S8. (a) Linear relationship between absorption and concentration of Au and Zn^{2+} from the diluted ICP solution based on the Beer-Lambert's law. (b) UV-vis absorption spectra of Au NRs and two hybrids in aqueous solution.

8. Beer-Lambert’s law for the concentration evaluation

The concentrations of Au NRs and ZnTPP were evaluated via Beer-Lambert's law (theoretical calculation) and inductive coupled plasma-mass spectroscopy (ICP-MS) (experimental value). According to the Beer-Lambert's law, a linear relationship between absorption and concentration was obtained (Fig. S8), where the concentrations of Au and Zn^{2+} were distributed from 0 to 1 mM. In comparison with the UV absorption, the absorption of Au NRs in all the samples was calibrated to be consistent and corresponding concentration was 0.221 mM based on the Beer-Lambert’s Law. In the same way, the concentrations of Zn^{2+} were 0.052 mM and 0.089 mM for Au NR@ZnTPP and Au NR@PVP+ZnTPP, respectively. In the ICP-MS analysis of Au NR@ZnTPP and Au

NR@PVP+ZnTPP, the concentration of Au atom was 0.212 mM for Au NR@ZnTPP and 0.228 M for Au NR@PVP+ZnTPP. The concentration of ZnTPP was 0.059 mM for Au NR@ZnTPP and 0.099 mM for Au NR@PVP+ZnTPP. Thus, the initial concentration of the samples based on Au atom is 43 μg/mL (equal to 0.221 mM).

References

S1. L. Cheng, W. He, H. Gong, C. Wang, Q. Chen, Z. Cheng and Z. Liu, *Adv. Funct. Mater.,* 2013, **23**, 5893-5902.

S2. A. Gole and C. J. Murphy, *Langmuir,* 2008, **24**, 266-272.

S3. C. J. Orendorff and C. J. Murphy, *J. Phys. Chem. B,* 2006, **110**, 3990-3994.